

Geophysical Research Letters®



RESEARCH LETTER

10.1029/2021GL097511

Key Points:

- El Niño–Southern Oscillation (ENSO) teleconnection changes are found over ~50% of teleconnected regions in December–February for the period 2081–2100, relative to 1950–2014
- The large majority of these projected teleconnection changes suggest that an amplification of the historical teleconnections will occur
- ENSO teleconnection changes largely scale with the projected warming level (i.e., higher warming leads to larger teleconnection changes)

Supporting Information:

Supporting Information may be found in the online version of this article.

Correspondence to:




S. McGregor,
shayne.mcgregor@monash.edu

Citation:

McGregor, S., Cassou, C., Kosaka, Y., & Phillips, A. S. (2022). Projected ENSO teleconnection changes in CMIP6. *Geophysical Research Letters*, 49, e2021GL097511. <https://doi.org/10.1029/2021GL097511>

Received 17 DEC 2021
Accepted 12 MAY 2022

Projected ENSO Teleconnection Changes in CMIP6

Shayne McGregor^{1,2} , Christophe Cassou³, Yu Kosaka⁴ , and Adam S. Phillips⁵ 

¹School of Earth Atmosphere and Environment, Monash University, Melbourne, VIC, Australia, ²ARC Centre of Excellence for Climate Extremes, Monash University, Melbourne, VIC, Australia, ³CERFACS/CNRS, Toulouse, France, ⁴Research Center for Advanced Science and Technology, University of Tokyo, Tokyo, Japan, ⁵National Center for Atmospheric Research, Boulder, CO, USA

Abstract The El Niño–Southern Oscillation (ENSO) has far reaching impacts through atmospheric teleconnections, which make it a prominent driver of global interannual climate variability. As such, whether and how these teleconnections may change due to projected future climate change remains a topic of high societal relevance. Here, ENSO Surface Temperature (TAS) and Precipitation (PR) teleconnections between the historical and high-emission future simulations are compared in more than 31 models from Phase 6 of the Coupled Model Intercomparison Project. We find significant future (2081–2100) TAS and PR teleconnection changes over approximately 50% of teleconnected regions in December–February relative to 1950–2014. The large majority of these significant teleconnection changes suggest that an amplification of the historical teleconnections will occur, however, some regions also display a significant teleconnection dampening. Further to this, in many regions these ENSO teleconnection changes scale with the projected warming level, with higher warming leading to larger teleconnection changes.

Plain Language Summary The El Niño–Southern Oscillation (ENSO) has far reaching impacts through atmospheric teleconnections, which make it a prominent driver of global interannual climate variability. As such, whether and how these teleconnections may change due to projected future climate change remains a topic of high societal relevance. Here, ENSO surface temperature (TAS) and precipitation (PR) teleconnections between the historical and high-emission future simulations from Phase 6 of the Coupled Model Intercomparison Project are compared. Focusing on the season when ENSO typically peaks (December–February), we find significant future (2081–2100) TAS and PR teleconnection changes over approximately half of teleconnected regions relative to 1950–2014. The large majority of these significant teleconnection changes suggest that an amplification of the historical teleconnections will occur, however, some regions also display a significant teleconnection dampening. Further to this, in many regions these ENSO teleconnection changes scale with the projected warming level. This scaling of teleconnection changes with warming suggests that a lot of the changes to ENSO teleconnections can be avoided by minimizing future warming, or vice versa, larger year to year TAS and PR variability due to ENSO is likely to be experienced with strong future warming.

1. Introduction

The term, El Niño–Southern Oscillation (ENSO), is used to describe variations between warm (El Niño) and the cool (La Niña) phases of anomalous Sea Surface Temperatures (SSTA) in the central and eastern equatorial Pacific and overlying changes in the atmospheric circulation. These events are also associated with large changes in tropical Pacific rainfall that are largely considered to be a redistribution of climatological Precipitation (PR) (Choi et al., 2015). The climatic impacts of ENSO though, are not restricted to the tropical Pacific. These climatic impacts, which are known as teleconnections, extend around the globe making ENSO the most prominent driver of global interannual climate variability (McPhaden et al., 2006; Taschetto et al., 2020). Some of the more remote teleconnections include temperature and PR changes as far away as South Africa and Antarctica (Taschetto et al., 2020).

The prominent global climate impacts of ENSO and its teleconnections make understanding any projected changes to anthropogenically induced warming extremely important. As such, it has been the area of much research in recent decades, since climate models utilized for projections began to realistically represent ENSO (Meehl et al., 1993; Timmermann, 1999). Previous generations (i.e., versions 5 and below) of Coupled Model Intercomparison Project (CMIP) models have shown no consensus on ENSO SSTA amplitude change in conventionally defined regions of the central-eastern equatorial Pacific (Cai et al., 2021; Eyring et al., 2021), however,

© 2022. The Authors.

This is an open access article under the terms of the Creative Commons Attribution-NonCommercial-NoDerivs License, which permits use and distribution in any medium, provided the original work is properly cited, the use is non-commercial and no modifications or adaptations are made.

signs of SST spatial structure changes were apparent (Power et al., 2013). The 6th installment of CMIP models (CMIP6) appear to display a slight increase in ENSO SSTA amplitude that is reported as insignificant when analyzed in 30 years windows (Lee et al., 2021), but significant when the entire 21st century is contrasted against the 20th century (Cai et al., 2022).

CMIP models do, however, display a relatively large enhancement and eastward shift of the tropical atmospheric response to ENSO, regardless of any ENSO SSTA amplitude changes (Cai et al., 2014; Lee et al., 2021; Power et al., 2013). As PR changes are often used to identify extreme ENSO events, these relative PR changes have underpinned projections of increasing extreme ENSO events in the future (Cai et al., 2014). As this PR enhancement is associated with an enhanced diabatic heating, which acts as a source of the atmospheric waves responsible for these teleconnections, the relative climatic impacts of ENSO events are expected to be larger (Cai et al., 2014). In CMIP5 models, however, the teleconnection changes have been more difficult to show simply at the grid point level than envisioned (Perry et al., 2017; Yeh et al., 2018), with supporting evidence instead coming from regional averages (Perry et al., 2020; Power & Delage, 2018) or the separation of climate models into subsets based on the representation of various factors (Bonfils et al., 2015; Cai et al., 2021).

CMIP6 models provide another opportunity to analyze the response of ENSO teleconnections to numerous prescribed radiative forcing scenarios across the new generation of state-of-the-art climate models (Eyring et al., 2016). Here, we add to the literature on projected ENSO teleconnection changes in CMIP6 models (Yeh et al., 2022), focusing on addressing the following question: “Do CMIP6 models agree on if and how global ENSO teleconnections will change under different projected emissions scenarios?”

2. Models and Methods

2.1. CMIP6 Models

Our CMIP6 analysis focuses on the projected change in PR and Surface Temperature (TAS) teleconnections over the period 2081–2100, with respect to the historical period simulation (1959–2014) under four different Shared Socioeconomic Pathways (SSP) (O’Neill et al., 2017). These are: SSP126, SSP245, SSP370 and SSP585, which respectively have an approximate global radiative forcing of 2.6, 4.5, 7.0, and 8.5 W/m² in the year 2100. We utilize all available models and ensemble members at the time of analysis (Table S1 in Supporting Information S1). We expect any impact of internal decadal variability on the multi-model ensemble mean (MMM) to be very small as it scales with 1/N, where N is the number of simulations utilised (e.g., Liguori et al., 2020).

Since the models all have a different number of ensemble members, for a comparison that does not weight a subset of models with more ensemble members more than other models, MMMs are calculated from model means where the individual models have more than one ensemble member. This ensures that each model has the same weighting in the MMM. It is worth noting that the results presented here are very similar if instead of using individual model means to calculate the ensemble mean, the first ensemble member of each individual model is used.

2.2. Methods

Here, each model's ENSO teleconnections are defined by linear regressions with the respective Nino 3.4 region SSTA (hereafter NINO34) at each grid point. This study focuses on the Surface Temperature (TAS) and PR teleconnections occurring during the typical ENSO peak phase during December–February (DJF). The statistical significance of the scenario ENSO teleconnection differences at each grid point, relative to the historical period, is calculated using a two-sample *t*-test. We note that only models that provide data in both experiments (i.e., the SSP scenario and historical simulation) are utilized in the difference and significance calculations (Table S1 in Supporting Information S1).

Regions utilized for the regional analysis presented here follow those defined for IPCC AR6 (Figure 1a and Table S2 in Supporting Information S1) (Iturbide et al., 2020). In regards to the regions, only land regions in which the MMM displays a significant teleconnection in at least one experiment (i.e., the SSP scenarios or historical simulations) are analyzed. Here, significant regional teleconnections are identified where the multi-model ensemble displays a teleconnection deemed significantly (at or above the 95% level) different from zero with a *t*-test.

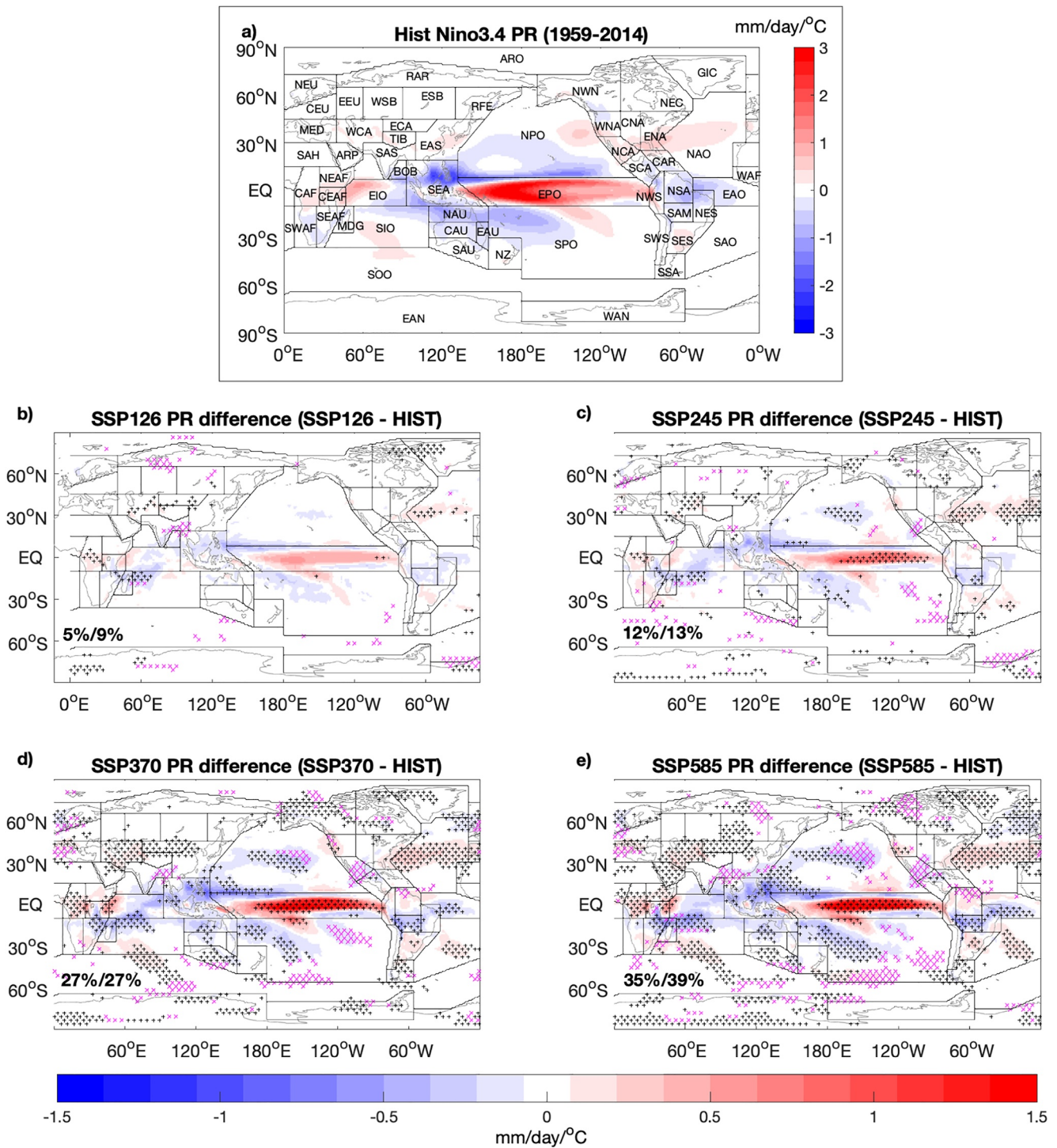


Figure 1. The global December–February precipitation (PR) teleconnections of El Niño–Southern Oscillation (ENSO) (measured in °C of the ENSO index) and their projected changes. (a) Displays the MME PR teleconnections of the historical simulation, calculated over the 1950–2014 period. The AR6 regions with region codes are overlaid (see Table S2 in Supporting Information S1). (b) through to (e) display the projected teleconnection changes in the 2081–2100 period for SSP-126 to SSP-585 scenarios (see panel titles). In panels (b–e), black stippling indicates projected statistical significant teleconnection amplification, while purple stippling indicates projected statistical significant teleconnection dampening. Numbers displayed in the bottom left of panels (b–e) represent the percentage global area (left) and global land area (right) displaying significant changes.

2.3. CMIP6 Representation of ENSO Teleconnections

Given the impact of these teleconnections on climate and extremes around the globe, it is important to understand how well they are reproduced in CMIP models. There are many ways to assess the model performance, including looking at simplified metrics like the agreement in the sign of the teleconnections (Langenbrunner & Neelin, 2013), regional average teleconnection strength over land (Perry et al., 2020), or a combination of both (Power & Delage, 2018). Simplified metrics like these suggest that CMIP6 models provide a robust depiction of the teleconnection representation (Eyring et al., 2021).

More complex metrics, like spatial correlation coefficients, have some drawbacks if you are trying to ascertain the skill of a particular model with limited ensemble members as they can be significantly influenced by climatic noise (Batehup et al., 2015; Perry et al., 2020). These spatial metrics are, however, well suited for looking at changes in multi-model mean properties, the focus of this study. The recent study of Planton et al. (2020) suggests that the spatial correlations at the near global scale (i.e., minus the tropical Pacific) between CMIP6 models and the observations are significantly stronger than those of CMIP5 models. As such, CMIP6 models appear to be a suitable tool to further explore projected future changes.

3. Projected Precipitation Teleconnection Changes

3.1. Global Precipitation (PR)

Significant differences are seen between projected ENSO teleconnections and historical simulations under all projection scenarios presented (Figures 1b–1f). As the central/eastern equatorial Pacific PR increases fall in the region with a relatively small positive ENSO PR teleconnection (Figure 1a), this PR change is consistent with the eastward shift of ENSO's equatorial PR response reported in earlier studies (e.g., Yun et al., 2021). There is also a remarkable visual similarity in the regions displaying projected teleconnection changes for each emissions scenario (Figures 1b–1f), which is reflected by the spatial correlations between difference maps ranging between 0.85 and 0.95 (Table S3 in Supporting Information S1). The magnitude of these teleconnection difference does, however, scale with the magnitude of the SSP scenarios radiative forcing (Figures 1 and S1a in Supporting Information S1) and the warming level in many locations (Figure S2a in Supporting Information S1). This is also reflected by the Root Mean Squared (RMS) scenario PR teleconnection differences being 0.068, 0.099, 0.176 and 0.174 mm/day/°C, respectively, for the SSP-126, 245, 370 and 585 scenarios (Figure 1).

Focusing on land areas, each projection scenario displays significant PR teleconnection changes. The smallest land area displaying these significant changes is approximately 9%, in the SSP-126 scenario projections, while the SSP-585 scenario displays significant teleconnection differences over approximately 39% of global land areas. The large majority of these significant teleconnection changes are amplifications of the historical teleconnections, as indicated by the large proportion of back stippling in Figures 1b–1e compared to the purple stippling.

3.2. Regional Precipitation (PR)

Our regional analysis finds significant projected changes in many of the regions (Figure 2), while also again suggesting that the number of regions expecting to see this change increases as the SSP scenario radiative forcing increases (Figure S1c in Supporting Information S1). For instance, for the SSP-126 scenario, only two regions display significant changes, with both suggesting an amplification of the regional teleconnection modeled during the historical period. While, for the high emission SSP-585 scenario, significant PR teleconnection changes are found in 20 regions. So approximately 49% of the regions that display a significant PR teleconnection display a significant SSP induced change. Furthermore, 19 of these 20 regions display a significant amplification of the historical period teleconnection, while the remaining region displays a significant dampening.

There are several regions that best display the apparent scaling of the teleconnection changes with increasing global warming levels (Figure S3 in Supporting Information S1). For a teleconnection amplification, the South American monsoon region (SAM), South-east South America, Mediterranean region and the western central Asia region are among those regions that display clear changes that appear to scale with forcing magnitude and warming level (Figures 2 and S3 in Supporting Information S1). On the other hand, regions like North Central

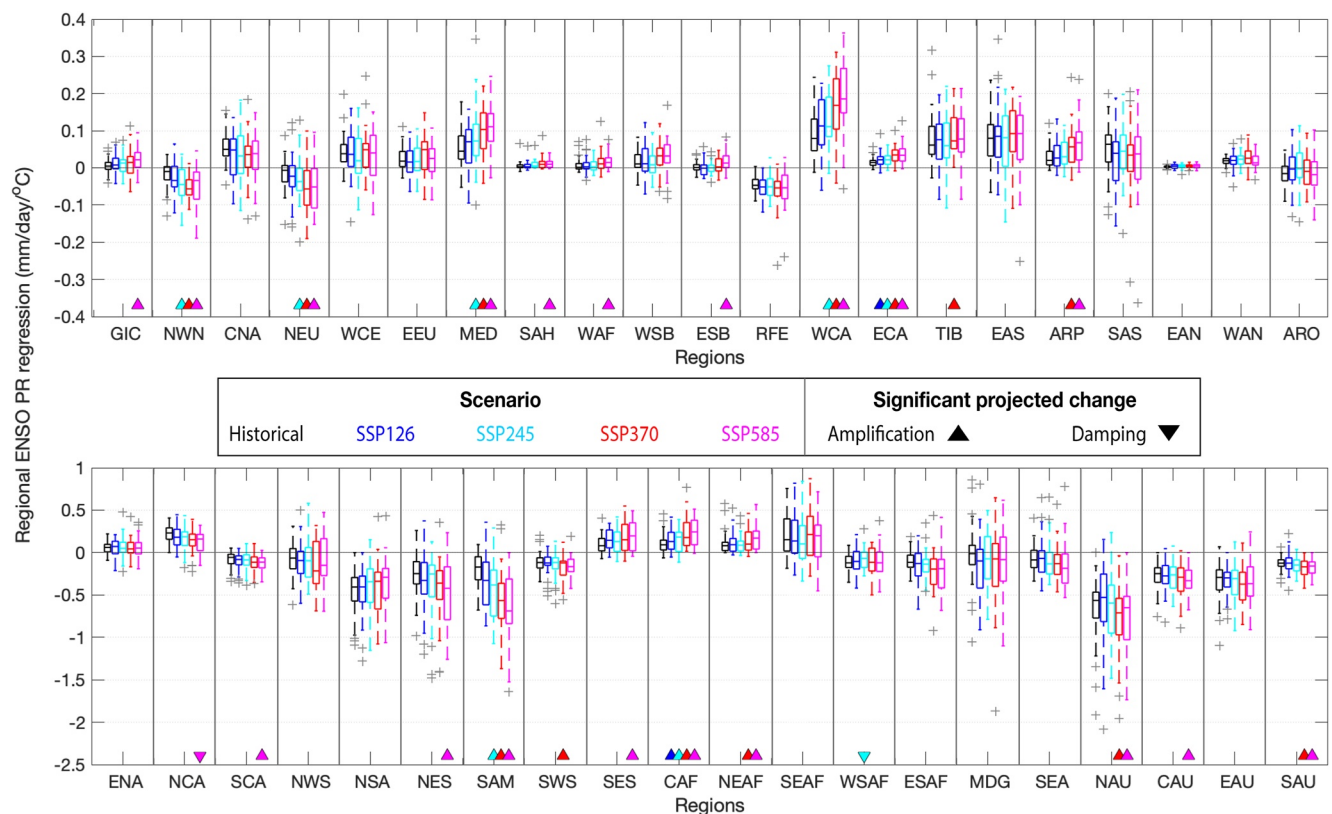


Figure 2. Regional precipitation (PR) teleconnections and their projected changes, where relatively low (high) PR teleconnection regions are presented in the upper (lower) panel (i.e., note the different y-axis values). Regional teleconnections of the different projections scenarios are depicted by the colors (See legend), while the historical teleconnections are represented by the black boxplots. Significant regional projected differences (at the 95% level) are identified by a colored symbol near the lower x-axis, where the colors again represent the scenario displaying the significant change, while the symbol indicates whether the change is an amplification or damping of the historical teleconnection (see legend). The central mark in each boxplot is the median, while the edges of the box are the 25th and 75th percentiles. Boxplot whiskers extend to the most extreme datapoints the algorithm considers to be not outliers, while the outliers are plotted individually (gray plus signs).

America (NCA) display a clear decreasing teleconnection strength with increasing radiative forcing and warming level.

4. Projected Surface Temperature Teleconnection Changes

4.1. Global Surface Temperature (TAS)

Significant differences are also clearly seen between projected ENSO TAS teleconnections (2081–2100) and historical simulations (Figure 3a; 1950–2014) in all projection scenarios presented (Figures 3b–3f). Similar to PR change, there is a very strong visual similarity between the projected teleconnection changes for each emissions scenario which is reflected by the spatial correlations between difference maps that range between 0.68 and 0.87 (Table S3 in Supporting Information S1). Consistent with what was seen for the PR teleconnection changes, the magnitude of these maps of teleconnection differences appears to scale with the magnitude of the SSP scenarios radiative forcing (Figures 3 and S1b in Supporting Information S1) and the global warming level (Figure S2b in Supporting Information S1). This is also seen in the RMS scenario TAS teleconnection differences of the SSP-126 scenario being $0.057^{\circ}\text{C}/^{\circ}\text{C}$, while the RMS of SSP-245, 370 and 585 scenarios are approximately 22%, 58% and 92% larger.

Focusing on land areas alone, each projection scenario again displays significant TAS teleconnection changes. The SSP-126 scenario projections display the smallest land area with significant changes, which is approximately 12%, while the SSP-585 scenario displays significant teleconnection differences over approximately 37% of global land areas.

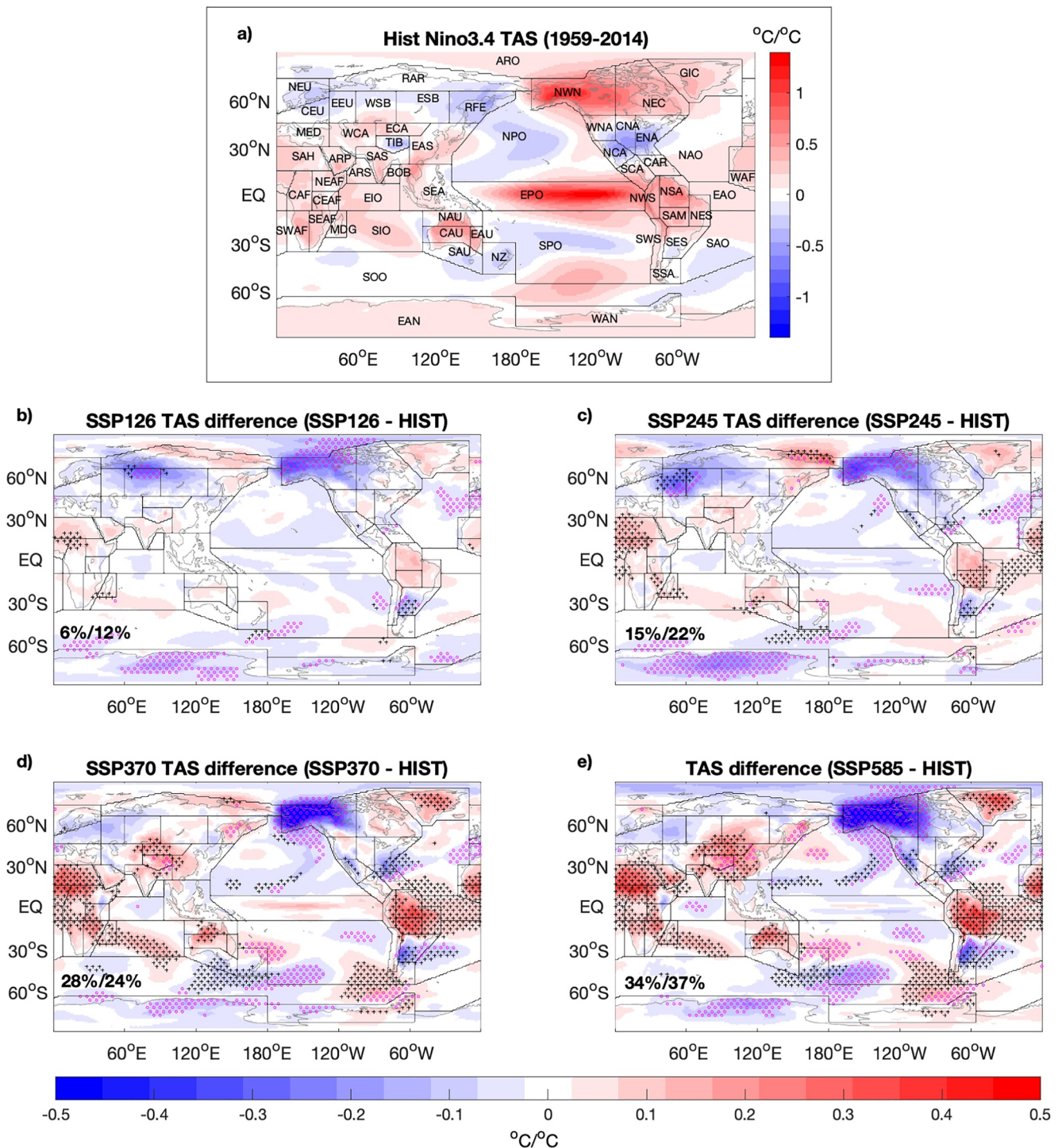


Figure 3. As in Figure 1, but for the global December–February surface temperature teleconnections of El Niño–Southern Oscillation and their projected changes.

4.2. Regional Temperature (TAS)

Regional analysis finds significant projected TAS teleconnection changes in many of the regions that display significant ENSO teleconnections (Figure 4). Further to this, these results again also suggest that the number of regions expecting to see this change increases as the scenario radiative forcing increases (Figure S1d in Supporting Information S1). For instance, the SSP-126 scenario has only two regions with significant changes, and both

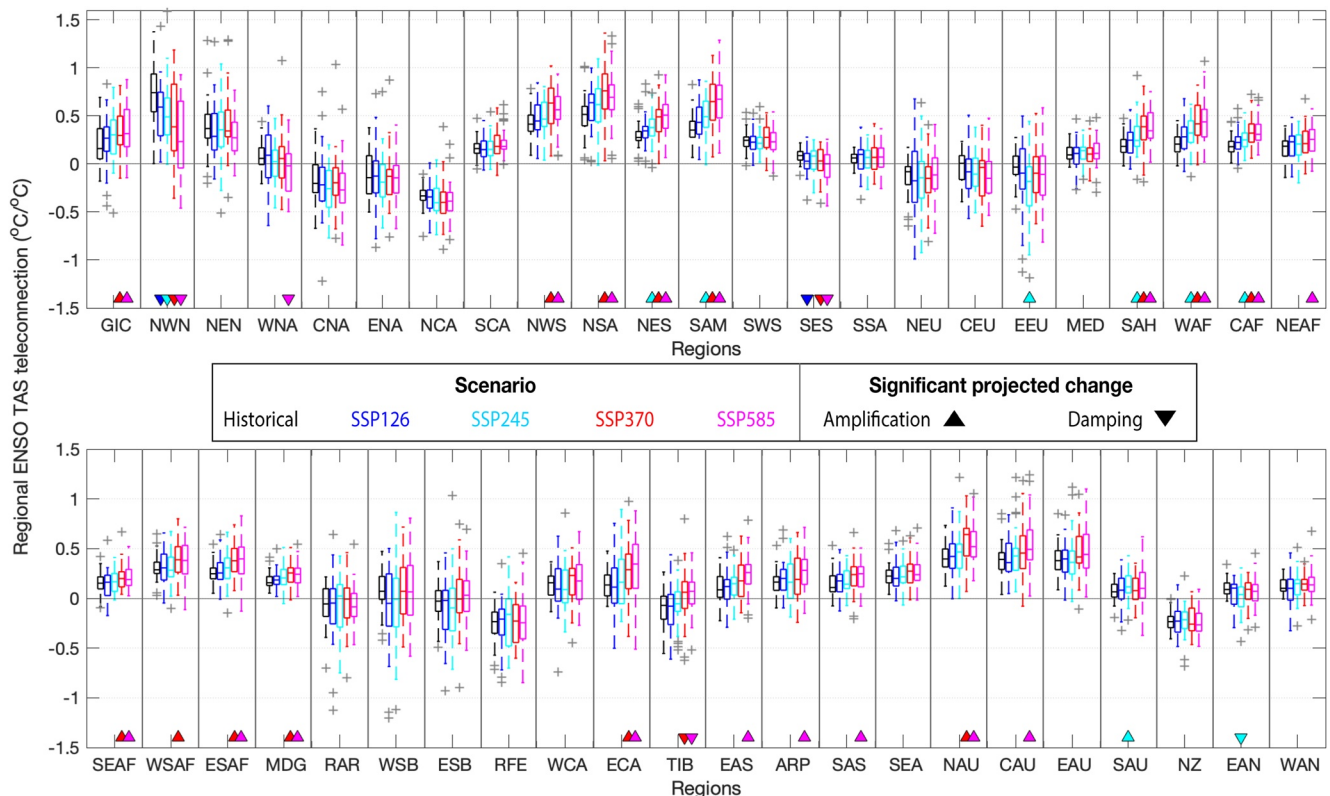


Figure 4. As in Figure 2, but for the regional surface temperature teleconnections and their projected changes.

of these display a dampening of the teleconnection modeled during the historical period. The high emission SSP-585 scenario, on the other hand, displays significant TAS teleconnection changes in 22 regions, accounting for 49% of the regions defined here to display an ENSO teleconnection. Eighteen of these regions display an amplification of the historical period teleconnection, while the remaining four regions display a dampening.

There are several regions that best display the apparent scaling of these TAS teleconnections changes with increasing warming levels. For teleconnection amplifications, the regions that occupy the Northern half of South America (e.g., North-west South-America, North South-America, North-east South-America, and the SAM) all seem to display a clear teleconnection amplification. There is, however, a temperature teleconnection amplification seen in many locations, including many regions in African, Australian and Asia. On the other hand, North West North-America and the Tibetan Plateau both display a clear decreasing TAS teleconnection strength with increased radiative forcing (Figure 4) and warming levels (Figure S4 in Supporting Information S1).

5. Mechanisms of Change/Amplification

Here we identify a clear eastward shift and intensification of the equatorial PR signal, which is consistent with many earlier studies (e.g., Yun et al., 2021). As to how this relates to the larger scale atmospheric circulation, we look to the velocity potential in the upper atmosphere (300 hPa level). A positive NINO34 SSTA is associated with a decrease in convergence over the central/eastern Tropical Pacific, and an increase in convergence over the tropical Indian and Atlantic oceans (Figure 5a, contours). As the SSP scenario forcing increases, a clear eastward shift of this velocity potential response is also clearly seen (Figures 5b and S5 in Supporting Information S1), such that the SSP585 scenario velocity potential pattern has a maximum spatial correlation with the historical pattern when it is shifted west by 12° longitude. This projected eastward shift leads to ENSO velocity potential teleconnection dampening over the western tropical Pacific, the western tropical Atlantic and over tropical South America, along with an amplification in most other tropical regions (Figures 5b and S5 in Supporting Information S1). The magnitude of this velocity potential response also appears to largely increase along with the eastward shift, such that the velocity potential teleconnection in the SSP585 scenario is ~25% stronger than

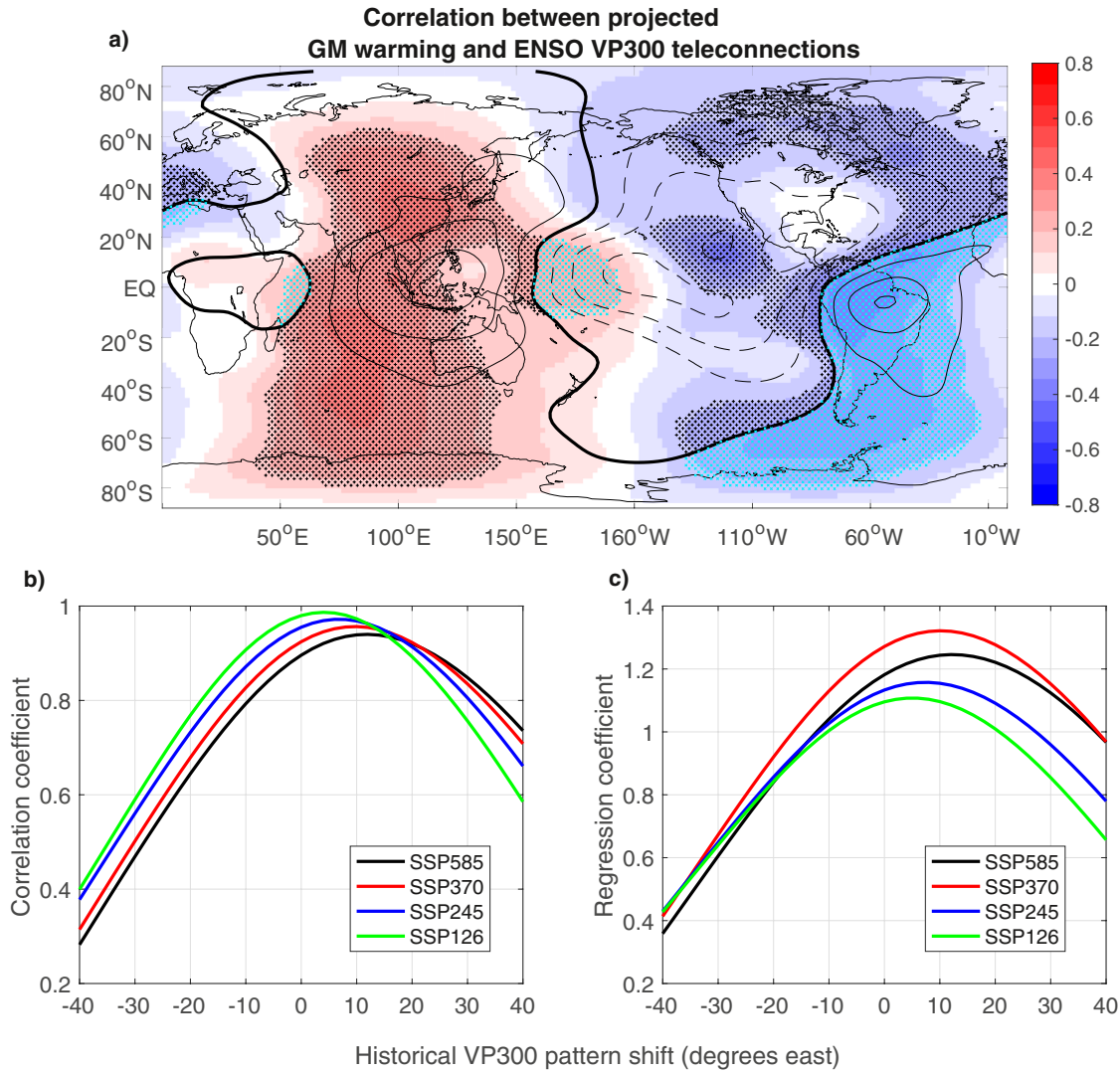


Figure 5. (a) Shading presents the correlation between each model's projected global mean warming (calculated as a difference between the 2080–2100 and 1958–2014 averages) and its El Niño–Southern Oscillation (ENSO) 300 hPa velocity potential teleconnection. The overlying black contours represent the historical ensemble mean ENSO 300 hPa velocity potential teleconnection. Black stippling indicates projected statistical significant teleconnection amplification, while cyan stippling indicates projected statistical significant teleconnection dampening. (b and c) respectively display the spatial correlation and regression relationship calculated between the historical and projected (see legend) ENSO teleconnection calculated while shifting historical pattern (x -axis).

the historical when it is shifted west by 12° longitude (Figure 5c). These changes again scale with the magnitude of the projected warming, as indicated by the shading and stippling shown in Figure 5a. Here, the majority of latitudes between 40° – 160° E have a positive relationship with warming level, while those between 170° W and 30° E largely display a negative relationship with warming level. It is also interesting to note that the historical ENSO velocity potential response, which is largely asymmetric about the equator in the Atlantic region, appears to become more symmetric in a high emission scenario and warming level future (Figure S5 in Supporting Information S1).

6. Conclusions

We find a clear and significant ENSO teleconnection changes in DJF for the period 2081–2100, relative to 1950–2014. These changes are most clearly seen as an eastward shift and intensification of the atmospheric response to ENSO, as shown by the velocity potential changes reported in Figure 5. These global atmospheric circulation

changes are consistent with those expected, given the projected intensification of ENSO PR changes reported in earlier studies (Cai et al., 2014, 2021; Power et al., 2013).

The transfer of this atmospheric circulation response to changes in TAS and PR teleconnections is partially clouded by the more complex range of processes required to drive these teleconnections (e.g., Drouard & Cassou, 2019). In spite of this, however, we find a clear signal for both TAS and PR, where under the high emission SSP585 scenario, approximately 50% of the regions that display significant historical TAS and/or PR teleconnections show significant projected teleconnection differences. We note that correlations calculated between a scenarios projected regional PR and temperature teleconnection changes (i.e., comparing the MMM-historical difference in Figures 2 and 4 for each emission scenario) display weak negative correlations that are not statistically significant. This suggests that knowing regional PR teleconnection changes cannot be used to inform the TAS teleconnection changes, and vice versa. However, the overwhelming majority of these significant projected regional temperature and PR changes suggest that an amplification of the historical teleconnections will occur (Figure S2 in Supporting Information S1), a result that is largely consistent with the CMIP5 findings of Power and Delage (2018). Further to this, the relatively small projected ENSO variance increases produced by CMIP6 models (Cai et al., 2022; Lee et al., 2021 c.f., Figure 4.10) would be expected to further enhance the projected teleconnection amplification reported here, making to total impact of ENSO events even larger.

There are, however, several TAS and PR teleconnected regions that display a significant projected decrease in teleconnection strength under the high emission SSP585 scenario. For instance, a decreasing ENSO PR teleconnection is seen in the NCA, consistent with the study of Drouard and Cassou (2019). It is also important to note that decreasing TAS teleconnections are found in the North-western North-American and western North-American regions is consistent with earlier studies (Beverley et al., 2021; Kug et al., 2010). This teleconnection damping has been linked to the eastward shifted anomalous circulation changes over the North Pacific, rather than other differences, like the equator-to-pole temperature gradient (Beverley et al., 2021; Drouard & Cassou, 2019).

Given that teleconnections are defined relative to ENSO SSTA, the teleconnection changes identified here must be largely associated with changes in either ENSO SSTA spatial structure, or background state changes. The dynamics of these tropical Pacific PR response to ENSO events has been investigated in detail in several previous studies (Chung & Power, 2016; e.g., Power et al., 2013), with results showing that the changes in PR anomalies arise from a nonlinear interaction between unchanged ENSO-driven SSTA and the spatial varying background (global) warming.

Analysis of emissions scenarios between the low emission SSP-126 through to the high emission SSP-585, suggest that the ENSO PR and TAS teleconnection changes in many areas appear to scale with the modeled warming level (i.e., higher warming levels leads to larger teleconnection changes). This scaling of teleconnections with warming level is likely at least partly related to changes in atmospheric moisture content and changes in the magnitude of the spatially varying background warming (i.e., weakening of Pacific zonal and meridional equatorial SST gradients) (Cai et al., 2021; Power et al., 2013). We note that some measures seem to suggest that the teleconnection changes saturate between the SSP370 and SSP585 scenarios, but this is not consistent across all measures. This should be explored further in future work.

It is also important to note that despite the MMM regional teleconnections displaying relatively large changes under moderate and high emission futures in most regions with significant changes, it is currently unclear how easy these changes would be to see in the real world (i.e., which is broadly equivalent to single model realization) due to model-to-model spread in the teleconnection changes (Figures 2 and 4) and the large amount of internal teleconnection variability (Batehup et al., 2015). However, the relatively small teleconnection changes projected for low emissions futures along with the scaling of teleconnection changes with warming suggests that a lot of the changes to ENSO teleconnections can be avoided by minimizing future warming, or vice versa, larger year to year TAS and PR variability due to ENSO is likely to be experienced with strong future warming.

Data Availability Statement

All CMIP6 processed data analyzed in this study are freely available from the Monash Bridges data repository, which can be found here: <https://doi.org/10.26180/c.5844803>.

Acknowledgments

We acknowledge the World Climate Research Programme, which, through its Working Group on Coupled Modeling, coordinated and promoted CMIP6. We thank the climate modeling groups for producing and making available their model output, the Earth System Grid Federation (ESGF) for archiving the data and providing access, and the multiple funding agencies who support CMIP6 and ESGF. This material is based upon work supported by the National Center for Atmospheric Research, which is a major facility sponsored by the National Science Foundation under cooperative agreement 1852977. S. McGregor was supported with funding from the Australian Government via the Australian Research Council and the National Environmental Science Program. Y. Kosaka was supported by the Japanese Ministry of Education, Culture, Sports, Science and Technology (JPMXD0717935457). Open access publishing facilitated by Monash University, as part of the Wiley - Monash University agreement via the Council of Australian University Librarians.

References

- Batehup, R., McGregor, S., & Gallant, A. J. E. (2015). The influence of non-stationary teleconnections on palaeoclimate reconstructions of ENSO variance using a pseudoproxy framework. *Climate of the Past*, 11(12), 1733–1749. <https://doi.org/10.5194/cp-11-1733-2015>
- Beverley, J. D., Collins, M., Lambert, F. H., & Chadwick, R. (2021). Future changes to El Niño teleconnections over the North Pacific and North America. *Journal of Climate*, 34(15), 6191–6205. <https://doi.org/10.1175/JCLI-D-20-0877.1>
- Bonfils, C. J. W., Santer, B. D., Phillips, T. J., Marvel, K., Leung, L. R., Doutriaux, C., & Capotondi, A. (2015). Relative contributions of mean-state shifts and ENSO-driven variability to precipitation changes in a warming climate. *Journal of Climate*, 28(24), 9997–10013. <https://doi.org/10.1175/JCLI-D-15-0341.1>
- Cai, W., Borlace, S., Lengaigne, M., Van Rensch, P., Collins, M., Vecchi, G., et al. (2014). Increasing frequency of extreme El Niño events due to greenhouse warming. *Nature Climate Change*, 4(2), 111–116. <https://doi.org/10.1038/nclimate2100>
- Cai, W., Ng, B., Wang, G., Santoso, A., Wu, L., & Yang, K. (2022). Increased ENSO sea surface temperature variability under four IPCC emission scenarios. *Nature Climate Change*, 12(3), 228–231. <https://doi.org/10.1038/s41558-022-01282-z>
- Cai, W., Santoso, A., Collins, M., Dewitte, B., Karamperidou, C., Kug, J.-S., et al. (2021). Changing El Niño–Southern Oscillation in a warming climate. *Nature Reviews Earth & Environment*, 2(9), 628–644. <https://doi.org/10.1038/s43017-021-00199-z>
- Choi, K.-Y., Vecchi, G. A., & Wittenberg, A. T. (2015). Nonlinear zonal wind response to ENSO in the CMIP5 models: Roles of the zonal and meridional shift of the ITCZ/SPCZ and the simulated climatological precipitation. *Journal of Climate*, 28(21), 8556–8573. <https://doi.org/10.1175/JCLI-D-15-0211.1>
- Chung, C. T. Y., & Power, S. B. (2016). Modelled impact of global warming on ENSO-driven precipitation changes in the tropical Pacific. *Climate Dynamics*, 47(3), 1303–1323. <https://doi.org/10.1007/s00382-015-2902-9>
- Drouard, M., & Cassou, C. (2019). A modeling- and process-oriented study to investigate the projected change of ENSO-forced wintertime teleconnectivity in a warmer world. *Journal of Climate*, 32(23), 8047–8068. <https://doi.org/10.1175/JCLI-D-18-0803.1>
- Eyring, V., Bony, S., Meehl, G. A., Senior, C. A., Stevens, B., Stouffer, R. J., & Taylor, K. E. (2016). Overview of the coupled model Inter-comparison Project Phase 6 (CMIP6) experimental design and organization. *Geoscientific Model Development*, 9(5), 1937–1958. <https://doi.org/10.5194/gmd-9-1937-2016>
- Eyring, V., Gillett, N. P., Achuta Rao, K. M., Barimalala, R., Barreiro Parrillo, M., Bellouin, N., et al. (2021). Human influence on the climate system. In V. Masson-Delmotte, P. Zhai, A. Pirani, S. L. Connors, C. Péan, S. Berger, et al. (Eds.), *Climate change 2021: The physical science basis. Contribution of working group I to the sixth assessment report of the intergovernmental panel on climate change*. Cambridge University Press.
- Iturbide, M., Gutiérrez, J. M., Alves, L. M., Bedia, J., Cerezo-Mota, R., Gimenez, E., et al. (2020). An update of IPCC climate reference regions for subcontinental analysis of climate model data: Definition and aggregated datasets. *Earth System Science Data*, 12(4), 2959–2970. <https://doi.org/10.5194/essd-12-2959-2020>
- Kug, J.-S., An, S.-I., Ham, Y.-G., & Kang, I.-S. (2010). Changes in El Niño and La Niña teleconnections over North Pacific–America in the global warming simulations. *Theoretical and Applied Climatology*, 100(3), 275–282. <https://doi.org/10.1007/s00704-009-0183-0>
- Langenbrunner, B., & Neelin, J. D. (2013). Analyzing ENSO teleconnections in CMIP models as a measure of model fidelity in simulating precipitation. *Journal of Climate*, 26(13), 4431–4446. <https://doi.org/10.1175/JCLI-D-12-00542.1>
- Lee, J.-Y., Marotzke, J., Bala, G., Cao, L., Corti, S., Dunne, J. P., et al. (2021). Future global climate: Scenario-based projections and near-term information. In V. Masson-Delmotte, P. Zhai, A. Pirani, S. L. Connors, C. Péan, S. Berger, et al. (Eds.), *Climate change 2021: The physical science basis. Contribution of working group I to the sixth assessment report of the intergovernmental panel on climate change*. Cambridge University Press.
- Liguori, G., McGregor, S., Arblaster, J. M., Singh, M. S., & Meehl, G. A. (2020). A joint role for forced and internally-driven variability in the decadal modulation of global warming. *Nature Communications*, 11(1), 3827. <https://doi.org/10.1038/s41467-020-17683-7>
- McPhaden, M. J., Zebiak, S. E., & Glantz, M. H. (2006). ENSO as an integrating concept in Earth science. *Science*, 314(5806), 1740–1745. <https://doi.org/10.1126/science.1132588>
- Meehl, G. A., Branstator, G. W., & Washington, W. M. (1993). Tropical Pacific interannual variability and CO₂ climate change. *Journal of Climate*, 6(1), 42–63. [https://doi.org/10.1175/1520-0442\(1993\)006<0042:TPIVAC>2.0.CO;2](https://doi.org/10.1175/1520-0442(1993)006<0042:TPIVAC>2.0.CO;2)
- O'Neill, B. C., Kriegler, E., Ebi, K. L., Kemp-Benedict, E., Riahi, K., Rothman, D. S., et al. (2017). The roads ahead: Narratives for shared socioeconomic pathways describing world futures in the 21st century. *Global Environmental Change*, 42, 169–180. <https://doi.org/10.1016/j.gloenvcha.2015.01.004>
- Perry, S. J., McGregor, S., Gupta, A. S., & England, M. H. (2017). Future changes to El Niño–Southern Oscillation temperature and precipitation teleconnections. *Geophysical Research Letters*, 44(20), 10608–10616. <https://doi.org/10.1002/2017GL074509>
- Perry, S. J., McGregor, S., Gupta, A. S., England, M. H., & Maher, N. (2020). Projected late 21st century changes to the regional impacts of the El Niño–Southern Oscillation. *Climate Dynamics*, 54(1–2), 1–18. <https://doi.org/10.1007/s00382-019-05006-6>
- Planton, Y. Y., Guilyardi, E., Wittenberg, A. T., Lee, J., Gleckler, P. J., Bayr, T., et al. (2020). Evaluating climate models with the CLIVAR 2020 ENSO metrics package. *Bulletin of the American Meteorological Society*, 102(2), 1–57. <https://doi.org/10.1175/BAMS-D-19-0337.1>
- Power, S. B., Delage, F., Chung, C., Kociuba, G., & Keay, K. (2013). Robust twenty-first-century projections of El Niño and related precipitation variability. *Nature*, 502(7472), 541–545. <https://doi.org/10.1038/nature12580>
- Power, S. B., & Delage, F. P. D. (2018). El Niño–Southern oscillation and associated climatic conditions around the world during the latter half of the twenty-first century. *Journal of Climate*, 31(15), 6189–6207. <https://doi.org/10.1175/JCLI-D-18-0138.1>
- Taschetto, A. S., Ummenhofer, C. C., Stuecker, M. F., Dommenget, D., Ashok, K., Rodrigues, R. R., & Yeh, S.-W. (2020). ENSO atmospheric teleconnections. In M. J. McPhaden, A. Santoso, & W. Cai (Eds.), *El Niño southern oscillation in a changing climate* (p. 26). American Geophysical Union.
- Timmermann, A. (1999). Detecting the Nonstationary response of ENSO to greenhouse warming. *Journal of the Atmospheric Sciences*, 56(14), 2313–2325. [https://doi.org/10.1175/1520-0469\(1999\)056<2313:DTNROE>2.0.CO;2](https://doi.org/10.1175/1520-0469(1999)056<2313:DTNROE>2.0.CO;2)
- Yeh, S.-W., Cai, W., Min, S.-K., McPhaden, M. J., Dommenget, D., Dewitte, B., et al. (2018). ENSO atmospheric teleconnections and their response to greenhouse gas forcing. *Reviews of Geophysics*, 56(May), 77–117. <https://doi.org/10.1002/2017RG000568>
- Yeh, S.-W., Wang, G., Cai, W., & Park, R. J. (2022). Diversity of ENSO-related surface temperature response in future projection in CMIP6 climate models: Climate change scenario versus ENSO intensity. *Geophysical Research Letters*, 49(4), e2021GL096135. <https://doi.org/10.1029/2021GL096135>
- Yun, K.-S., Lee, J.-Y., Timmermann, A., Stein, K., Stuecker, M. F., Fyfe, J. C., & Chung, E.-S. (2021). Increasing ENSO–rain–fall variability due to changes in future tropical temperature–rainfall relationship. *Communications Earth & Environment*, 2(1), 43. <https://doi.org/10.1038/s43247-021-00108-8>